







Intrinsic circularly polarized exciton emission in a twisted van der Waals heterostructure

J. Michl ¹, C. C. Palekar,² S. A. Tarasenko,³ F. Lohof ^{4,5}, C. Gies ^{4,5}, M. von Helversen,² R. Sailus ⁶, S. Tongay,⁶ T. Taniguchi,⁷ K. Watanabe,⁸ T. Heindel ², B. Rosa,² M. Rödel,⁹ T. Shubina,³ S. Höfling ¹, S. Reitzenstein,²

C. Anton-Solanas ^{1,10} and C. Schneider¹⁰

¹*Technische Physik, Physikalisches Institut and Wilhelm Conrad Röntgen-Center for Complex Material Systems, Universität Würzburg, Am Hubland, D-97074 Würzburg, Germany*

²*Institute of Solid State Physics, Technische Universität Berlin, D-10623 Berlin, Germany*

³*Ioffe Institute, 194021 St. Petersburg, Russia*

⁴*Institute for Theoretical Physics, University of Bremen, D-28334 Bremen, Germany*

⁵*Bremen Center for Computational Materials Science, University of Bremen, 28359 Bremen, Germany*

⁶*School for Engineering of Matter, Transport, and Energy, Arizona State University, Tempe, Arizona 85287, USA*

⁷*International Center for Materials Nanoarchitectonics, National Institute for Materials Science, 1-1 Namiki, Tsukuba 305-0044, Japan*

⁸*Research Center for Functional Materials, National Institute for Materials Science, 1-1 Namiki, Tsukuba 305-0044, Japan*

⁹*Experimentelle Physik 6, Universität Würzburg, Am Hubland, D-97074 Würzburg, Germany*

¹⁰*Institute of Physics, Carl von Ossietzky University, 26129 Oldenburg, Germany*



(Received 20 May 2021; revised 25 March 2022; accepted 18 May 2022; published 13 June 2022)

We report the emergence of a significant degree of intrinsic circular polarization of exciton photoluminescence in a twisted MoSe₂/WSe₂ heterostructure upon nonresonant driving with a linearly polarized laser. The effect is not related to the polarization of the incident light. Moreover, it is present at zero magnetic field, and reacts perceptibly to a perpendicularly applied magnetic field that, unexpectedly, can strongly diminish this effect. The giant magnitude of the polarization, which cannot be explained by natural optical activity or circular dichroism of the twisted lattice, suggests a kinematic origin arising from an emergent pyromagnetic symmetry in our structure, which we exploit to gain insight into the microscopic optical processes of our device.

DOI: [10.1103/PhysRevB.105.L241406](https://doi.org/10.1103/PhysRevB.105.L241406)

I. INTRODUCTION

Controlling the polarization of the emitted light in layered semiconductor structures is a delicate task in solid-state photonics, being of greatest importance in optoelectronic applications. The most known device to control the polarization of light is the standard wave plate, whose working principle relies on the effect of optical birefringence in anisotropic materials. However, most transparent materials used for such optical or near infrared applications have limited optical anisotropy, rendering waveplates inherently bulky and unsuitable for microscale photonic integration. More recently, it was found that nanostructures [1], microcavities [2], and photonic crystal slabs with chiral symmetry [3,4] cause strong polarization of light from unpolarized emitters. Thus, it became possible to realize nano- and microlasers [5], which intrinsically feature a strong degree of circular polarization without the need for external magnetic fields. The circular polarization effect in such chiral structures is based on a special engineering of the electromagnetic field in photonic cavities with reduced symmetry, for example, by forming polarizing patterns based on, e.g., gammadions-shaped elements [6]. However, the lateral dimensions of these patterned structures are still too large for next-generation integrated photonics.

Recently, much attention has been paid to the study of atomically thin transition metal dichalcogenides (TMDCs),

since they can absorb up to 10% of incident light at less than 1-nm thickness [7]. Monolayers of TMDCs have unique optical properties, such as the locking of spin and valley degree of freedom, which arises from the combination of broken inversion symmetry and strong spin-orbit coupling [7]. The selection rules reveal that the emission is circularly polarized if a particular spin/valley is selectively populated by circularly polarized pump light or in an external magnetic field. In the context of this paper, it is noteworthy that without the application of magnetic fields and under a linearly polarized or unpolarized pump, the photoluminescence of two-dimensional (2D) TMDC monolayer crystals does not exhibit any degree of circular polarization (DCP).

In this work, in turn, we investigate whether a van der Waals heterostructure composed of two different TMDC layers can efficiently convert linearly polarized or unpolarized light into light featuring a significant degree of circular polarization. Our experiment, which is carried out using a twisted bilayer of MoSe₂/WSe₂, reveals compelling features of elliptical polarization generated by Moiré excitons. Surprisingly, we observe a DCP orders of magnitude larger than $\sim d/\lambda$, expected from the circular dichroism of such a chiral stack [8], where d is the bilayer thickness and λ is the light wavelength. Our analysis suggests a kinetic origin of exciton circular polarization. The developed theoretical model predicts a DCP of up to 50% in agreement with the maximal experimental DCP of 0.44 ± 0.02 , which we detect in our studies.

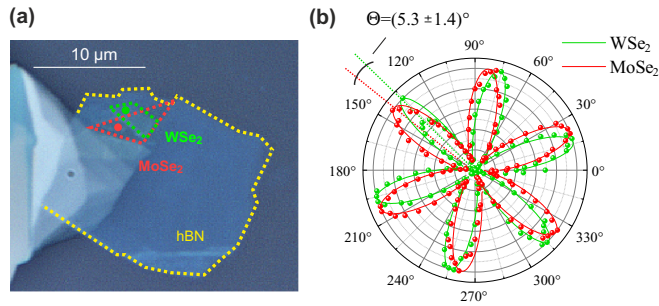


FIG. 1. Description of the sample and determination of the heterostructure twist angle. (a) Microscope image of the sample, the hBN/WSe₂/MoSe₂ flake limits are marked in a dashed yellow/green/red line. (b) Linear polarization analysis of the second harmonic generated light from freestanding monolayer regions of WSe₂ and MoSe₂ (see green and red dots in panel (a), respectively, where the measurements are performed). The polar plots correspond to the normalized intensities versus the analyzed linear polarization orientation. The twist angle is $(5.3 \pm 1.4)^\circ$.

II. EXPERIMENTAL RESULTS

We utilize the dry stamping method [9] in a home-built microscope to assemble the van der Waals heterostructure composed of a nominally 10-nm thin layer of hexagonal boron nitride (hBN, deposited on a SiO₂ substrate, see dashed yellow line depicting the limits of the hBN sheet), a monolayer of MoSe₂ and a final WSe₂ monolayer. The corresponding green and red areas in Fig. 1(a) outline the monolayers (the vertical stacking order is sketched in Fig. S2).

The twist angle between the two WSe₂/MoSe₂ sheets is determined by second harmonic generation measurements at room temperature [10]. We use a tunable mode locked laser (1480 nm) that excites isolated WSe₂ and MoSe₂ regions (positions indicated in Fig. 1(a) by a green and red dots, respectively) with a linear polarization oriented at a tunable angle φ . The second harmonic generated signal at

740 nm (1.676 eV) is detected as a function of the angle φ of the incoming laser linear polarization, yielding the polar plot shown in Fig. 1(b). The slight rotation between the two SHG polarization-dependent intensities reveals the twist angle $\theta = (5.3 \pm 1.4)^\circ$ between the WSe₂ and MoSe₂ layers. Importantly, we note that this angle can locally vary upon the formation of domains with lowered symmetry [11]. In addition, the 2H stacking of the heterostructure is confirmed by magneto-optical measurements (see Supplemental Material Fig. S5 [12]).

Having established the rotational alignment of the two atomically thin layers, next, we study the intrinsic optical properties of our system at cryogenic temperatures (1.8 K). We excite the sample with a 532-nm laser (focused on a spot size of 3 μ m diameter, 0.41 mW pump power), and collect the emitted photoluminescence (PL) over a broad spectral range. The objective has a numerical aperture of 0.81. Figure 2(a) shows the PL spectrum, characterized by two sets of pronounced features arising from the interlayer indirect exciton (IX, energy emission around 1.30–1.40 eV) and the intralayer excitons (around 1.60–1.70 eV).

The intralayer luminescence from both MoSe₂ and WSe₂ excitons is composed of neutral and charged excitonic complexes. In contrast, at lower emission energies we observe a distinct multipeak signature that we attribute to interlayer excitons formed in the WSe₂/MoSe₂ heterobilayer [13,14].

To confirm the hypothesis of the formation of interlayer excitons by rapid carrier transfer between the two monolayers, we study the PL excitation (PLE) spectrum of the IX emission for excitation energies between 1.59 and 1.70 eV. The overall PLE intensities of the IX are determined by integration of the PLE spectra between 1.27 and 1.44 eV and they exhibit two maxima at ~ 1.62 and ~ 1.69 eV, see red dots in Fig. 2(a). The PLE was implemented with a tunable continuous wave laser, using a constant pump power of 5.0 μ W across all the scanning excitation energies. The PLE spectrum suggests efficient carrier separation within the heterobilayer and formation of IX complexes following both a photoinjected exci-

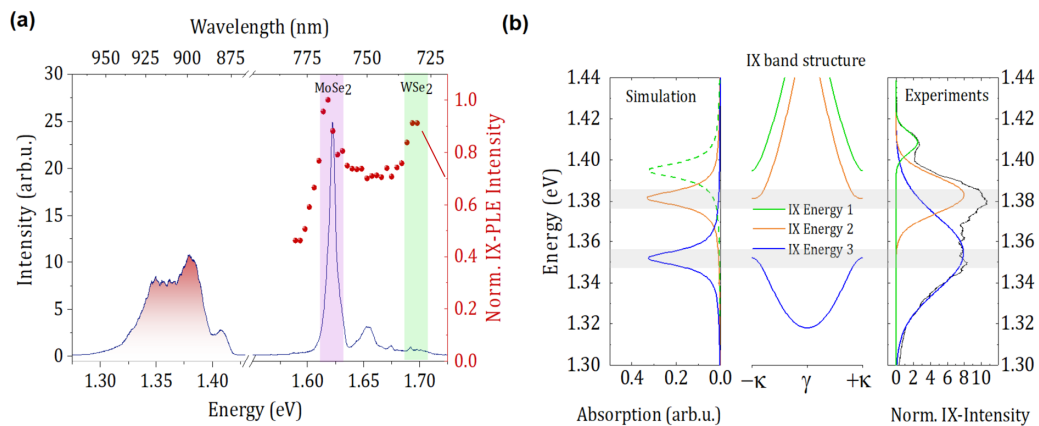


FIG. 2. Photoluminescence of intra- and interlayer excitons. (a) Comparison of low temperature photoluminescence of interlayer and intralayer (see labels WSe₂ and MoSe₂) excitons. The red dots (right vertical axis) represent the IX PLE spectrum, revealing two resonances (highlighted in a green and magenta band and spectrally resonant to the WSe₂ and MoSe₂-X energies, respectively) where carrier transfer occurs. (b) [left] Plot of the optical resonances obtained from the calculated band structure. [center] Corresponding IX band-structure. [right] Experimental spectrum reproduced from panel (a) presenting with Lorentzian fits, matching the resonance energies and dispersion at the K points of the corresponding reduced Brillouin zone.

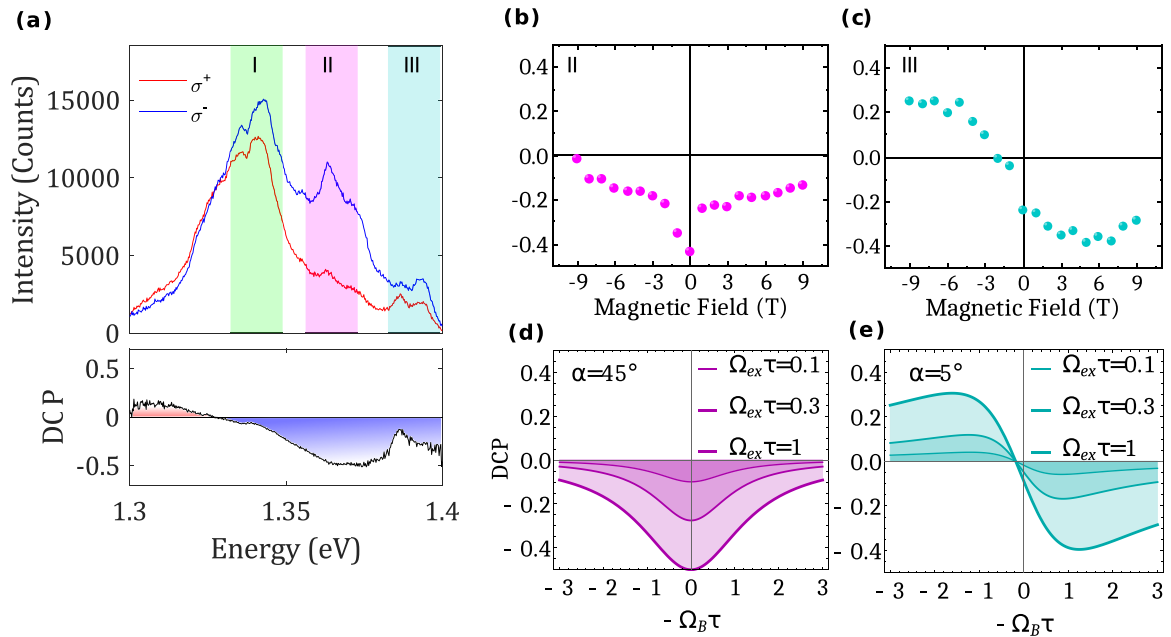


FIG. 3. Circular polarization analysis of the IX spectrum. (a) The sample is driven by a linear polarized laser, and luminescence is recorded under σ^+ and σ^- circular-polarization detection (orange and blue traces, respectively). The lower panel depicts the corresponding DCP as a function of the emission energy. Three energy regions I, II, and III are marked in green, magenta, and cyan colors. The laser excitation wavelength is 730 nm and the continuous wave pump power is $0.53 \mu\text{W}$, the measurement is taken under zero magnetic field. (b),(c) DCP dependence versus magnetic field from the energy regions II and III. The DCP values are averaged at each energy in a spectral interval of 20 meV around the marked energy regions. (d) and (e) DCP simulation of excitons as a function of $\Omega_B \tau$, represented according to Eq. (3) for the angles between the eigenframes of the UES and LES doublets $\alpha = 45^\circ$ and 5° and $\Omega_{ex} \tau = 0.1, 0.3, 1.0$ (see panel legends).

tation in the WSe_2 layer (hole tunneling) and the MoSe_2 layer (electron tunneling). Indeed, slight spectral shifts between the excitonic PL from the monolayers and the PLE resonances in $\text{WSe}_2/\text{MoSe}_2$ stacks have been observed [14,15] and can be attributed to renormalization phenomena related to dielectric screening and strain in the stacking procedure.

Earlier works have attributed the emergence of a multiplex structure in the PL signal of slightly rotated van der Waals heterostructures to the emergence of Moiré trapped excitons [13]. To support this interpretation in our sample, we model the energy spectrum of IX excitons in the presence of a Moiré potential using a low-energy continuum model [16,17], which we detail in the Supplementary section 1 [12].

In Fig. 2(b) we plot the IX Moiré exciton band structure as a function of momentum in the Moiré mini-Brillouin zone. At a rotation angle of 5° (similar to our experiments), we yield a set of optical resonances at K/K' that are separated by 20–40 meV [18]. For the identification of the resonances in the emission spectrum, we consider the selection rules based on dipole matrix elements for in-plane and out-of-plane polarization, according to which the lower two resonances are bright for normal incidence. We associate these resonances with the two lower-energy peaks in the measured PL spectrum in the right panel of Fig. 2(b). The third Moiré-exciton band emits mostly in the z polarization.

While the selection rules for Moiré excitons have been vastly investigated [13,19] and explain circularly polarized PL under circularly polarized laser driving, we are interested in the intrinsic possibility of twisted van der Waals heterostructures to emit light carrying a significant degree of circular

polarization without relying on the helicity of incident light. Therefore, we excite the system with a CW laser (excitation power $\sim 0.5 \mu\text{W}$, spot size $3 \mu\text{m}$ diameter) in the WSe_2 layer (730 nm), far above the IX band, using linearly polarized light, and analyze the DCP of the IX-PL emission.

In Fig. 3(a), we plot two PL spectra of the Moiré exciton band, detecting σ^+ and σ^- polarized light. The most remarkable feature is captured within the central PL peak located in region II. It clearly displays a predominance of the σ^- -polarized component. The observation is visualized by extracting the DCP, calculated as $(I_{\sigma^+} - I_{\sigma^-})/(I_{\sigma^+} + I_{\sigma^-})$, which is displayed in the bottom panel. For energies around 1.363 eV, the DCP value reaches a minimum value of $-(0.44 \pm 0.02)$.

To gain deeper insight in the polarization behavior of our sample, we acquire PL spectra at different magnetic fields and analyze the DCP. We subdivide the signal in three spectral regions I, II, and III, corresponding to the three assigned Moiré exciton peaks [see labels in Fig. 3(a) marked with colored rectangles]. The energy region I has a small intrinsic DCP for all tested magnetic fields (see Supplemental Material Fig. S3 for details [12]). We observe that the DCP attributed to the energy region III can be tuned by the magnetic field to change the DCP sign, see Fig. 3(c). In contrast, the central peak in region II, Fig. 3(b), behaves fundamentally different. The absolute DCP value is maximal for zero magnetic field and decreases independent of the sign of the applied magnetic field. The captured behavior remains qualitatively the same if the sample is driven with a pump wavelength of 768 nm, close to the MoSe_2 resonance, as shown in Fig. S4.

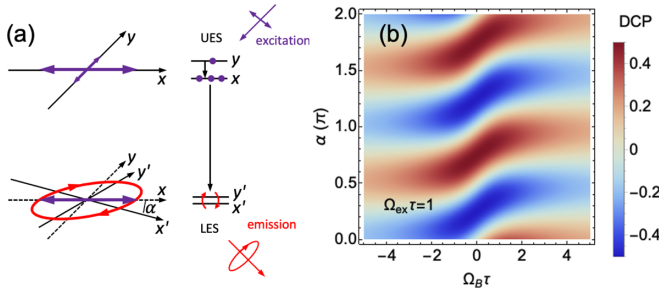


FIG. 4. Microscopic model of kinetic spin polarization of excitons. (a) Exciton alignment along x in the longitudinal-transverse-split upper exciton state (UES) followed by quantum beats in the rotated longitudinal-transverse-split lower exciton state (LES) leads to exciton spin polarization. (b) DCP simulation as a function of α (angle between the x and x' axes) and $\Omega_B \tau$ (spin precession frequency in the external magnetic field) for $\Omega_{ex} \tau = 1$.

III. DISCUSSION

The giant intrinsic circular polarization of the Moiré exciton emission observed in our experiment is surprising for nonmagnetic samples. Both, its magnitude, significantly exceeding the expected polarization resulting from a natural circular dichroism [8], and its unusual dependence on magnetic field, suggest a qualitatively different mechanism of exciton spin polarization.

A possible explanation for our results arises from a kinetic spin polarization of excitons in twisted TMDC heterobilayers: In analogy to the experimental conditions, we consider that excitons are optically injected into an upper exciton state (UES), relax into lower exciton state (LES), and then recombine emitting photons, as illustrated in Fig. 4(a). Like in our experimental conditions, the upper state is represented by the resonantly driven WSe₂ or MoSe₂ intralayer transition, which then relaxes to the IX state, which is the LES.

The upper exciton state consists of two sublevels corresponding to the excitons linearly polarized along orthogonal x and y axes [cf. the sketch depicted in Fig. 4(a)]. We assume that these sublevels are longitudinal-transverse split due to the anisotropic exchange interaction between electrons and holes [20–22], which can originate from local in-plane strain or structural imperfections and is known to be large in TMDC layers [23–27]. In the case of large splitting compared to the thermal energy and fast spin relaxation compared to the lifetime in the upper exciton state, excitons polarize along the x axis.

At the second step, linearly polarized excitons relax to the LES from which the light emission occurs, i.e., the IX state. The LES is also composed of a doublet consisting of two orthogonal linearly polarized exciton states. Importantly, in twisted bilayers, the eigenaxes of the LES doublet x' and y' do not coincide with the eigenaxes of the UES doublet. As a result, the excitons experience quantum beats in the lower-energy states inducing a circular polarization.

In the pseudospin representation, the average exciton polarization in the lower-energy state is described in the Poincaré sphere by the vector $s = \mathbf{S}/N$, where \mathbf{S} is the vector of the total exciton polarization and N is the number of excitons. The components $(s_x, s_y, s_z) = (DLP, DDP, DCP)$ describe the

Stokes polarization parameters of excitons: the linear polarization in the (x, y) plane, the linear polarization in the diagonals of the x and y axes, and the circular polarization, respectively. The vector \mathbf{S} satisfies the equation

$$\frac{d\mathbf{S}}{dt} = \boldsymbol{\Omega} \times \mathbf{S} + \mathbf{G} - \frac{\mathbf{S}}{\tau}, \quad (1)$$

where $\boldsymbol{\Omega} = (\Omega_{ex} \cos 2\alpha, \Omega_{ex} \sin 2\alpha, \Omega_B)$ is the effective Larmor frequency corresponding to the anisotropic exchange interaction and Zeeman splitting in the LES, $\Omega_{ex} = \Delta_{ex}/\hbar$, Δ_{ex} is the exchange splitting, α is the angle between the x and x' axes [see Fig. 4(a)], $\Omega_B = g\mu_B B/\hbar$ is the frequency of spin precession in the external magnetic field $\mathbf{B} \parallel z$, g is the effective exciton g factor, \mathbf{G} is the exciton polarization along x in the UES, $1/\tau = 1/\tau_0 + 1/\tau_s$, with τ_0 and τ_s the recombination time and spin relaxation time of excitons in the final state (LES), respectively. We do not consider thermalization of excitons in the lower state, since it does not lead to a build-up of circular polarization at zero magnetic field.

N is found from the equation $dN/dt = \Gamma - N/\tau_0$, where Γ is the exciton incoming from the upper to the lower state. The solution of Eq. (1) in the steady state has the form

$$\mathbf{S} = \frac{\tau \mathbf{G}^2 + \tau^2 \boldsymbol{\Omega} \times \mathbf{G} + \tau^3 \boldsymbol{\Omega} (\boldsymbol{\Omega} \cdot \mathbf{G})}{1 + \Omega^2 \tau^2}, \quad (2)$$

yielding the Stokes parameters of the excitonic emission. The DCP reads

$$\text{DCP} = \frac{-\Omega_{ex} \tau \sin 2\alpha + \Omega_{ex} \Omega_B \tau^2 \cos 2\alpha}{1 + (\Omega_{ex}^2 + \Omega_B^2) \tau^2} \frac{\tau}{\tau_0} P_0, \quad (3)$$

where $P_0 = G/\Gamma$ is the linear polarization of excitons in the upper state (the degree of linear/diagonal polarization, DLP/DDP, is given in the Supplemental Material [12]). The DCP sensibly depends on both the external magnetic field as well as the exchange interaction in the LES and the rotation of the eigenframes. To visualize this parameter space, we plot in Fig. 4(b) [Fig. S1 [12]] the DCP in a map versus the angle α and the frequency of spin precession in the external magnetic field (the frequency of exchange splitting) for a particular value $\Omega_{ex} \tau = 1$ [$\Omega_B \tau = 0$]. The DCP of excitons in the final state can be notable: In the optimal case of $P_0 = 1$, $\alpha = \pi/4$, $\Omega_{ex} \tau = 1$, and $\tau_0 \ll \tau_s$, as plotted in Fig. 3(d), the DCP reaches 50%. In the structures with $\alpha = \pi/4$, the DCP has a maximum at zero magnetic field and is suppressed by the field \mathbf{B} . This is furthermore evident in the representation in Fig. 3(d), which reproduces the fundamental behavior of the captured polarization of our Moiré excitons in the energy range 1.35–1.38 eV shown in Fig. 3(b).

In nonchiral structures, where $\alpha = 0$ or $\pi/2$, the DCP vanishes at zero magnetic field, rises with field at small fields, reaches a maximum at $\Omega_B \tau = 1$, and then decays, following the standard Lorentz curve. The field dependence of the spin polarization is thus controlled by the parameter $\Omega_B \tau$, and the spin polarization can be much higher than the thermal spin polarization controlled by the ratio between the Zeeman splitting and the thermal energy.

For intermediate conditions at slightly rotated eigenframes (e.g., 5°), we reach the scenario which is plotted in Fig. 3(e) well reproducing the polarization response of the high energy

peak in our spectrum, see Fig. 3(c). Here, we observe a modest DCP at zero magnetic field, which asymmetrically increases or inverts at negative/positive applied fields.

Our microscopic model also predicts that individual excitons have a finite DLP (see Supplemental Material 1b [12]). Note that the DLP of the PL collected from a macroscopic area can be much smaller than the DLP of a single site because of random orientation of the UES doublet. Circular polarization still survives since it is determined by the correlation between the nearby UES and LES duplets in the twisted structure rather than the absolute orientations of the UES duplets.

IV. CONCLUSION

The emergence of exciton spin polarization S_z in our van der Waals heterostructure in the absence of an external magnetic field \mathbf{B} and not related to the polarization of optical pump, is allowed by the C_3 point-group symmetry of heterobilayers. In this pyromagnetic group, the z component of an axial vector is invariant and, therefore, S_z may be created by an unpolarized pump. The effect also does not contradict time reversal symmetry: The spin polarization is formed here as a result of dissipative processes (energy and spin relaxation), which break time reversal symmetry, and would vanish at equilibrium [28,29]. Therefore, the kinetic spin polarization of excitons discussed here is fundamentally different from the optical effects related to spatial dispersion such as natural optical activity and circular dichroism, for which the photon wave vector plays a crucial role. The kinetic origin furthermore explains the observed DCP which reach notable experimental values exceeding 0.4 under conditions of retained time reversal symmetry.

As an interesting addition, we have experimentally verified in Fig. S6 that the effect can also be retained in the regime of tight Moiré trapping, where the IX spectrum breaks up in a discretized zoo of emission lines. This makes our scheme of interest for engineering the polarization of quantum emitters in atomically thin crystals and presents a clear strategy to engineer chiral materials and quantum light sources utilizing a twistrionics-based approach.

ACKNOWLEDGMENTS

We thank M. Florian, D. Erben, S. Kersch, and A.V. Poshakinskiy for useful discussions. We acknowledge funding via the priority program SPP2244 2DMP of the German Research Foundation (DFG), via Projects No. SCHN1376 14-1, No. RE2974/26-1, No. GI1121/4-1, and No. RTG2247 QM³ (graduate school program). F.L. is grateful for his support from the CRDF of the University of Bremen. S.A.T. acknowledges support by Russian Science Foundation (Grant No. 19-12-00051, theory). T.S. acknowledges support by Russian Science Foundation (Grant No. 19-12-00273; data analysis). S.T. acknowledges Grants No. DOE-SC0020653, No. DMR 2111812, No. DMR 1933214, No. DMR 1904716, and No. ECCS 2052527 for material development and integration. K.W. and T.T. acknowledge support from the MEXT Element Strategy Initiative to Form Core Research Center, Grant No. JPMXP0112101001 and JSPS KAKENHI Grant No. JP20H00354. T.H. acknowledges financial support by the German Federal Ministry of Education and Research (BMBF) via the QuSecure project (Grant No. 13N14876) within the Photonic Research Germany funding program. S.H. acknowledges funding via the DFG Grant HO 5194/16-1.

-
- [1] K. Konishi, M. Nomura, N. Kumagai, S. Iwamoto, Y. Arakawa, and M. Kuwata-Gonokami, Circularly Polarized Light Emission from Semiconductor Planar Chiral Nanostructures, *Phys. Rev. Lett.* **106**, 057402 (2011).
 - [2] A. A. Maksimov, I. I. Tartakovskii, E. V. Filatov, S. V. Lobanov, N. A. Gippius, S. G. Tikhodeev, C. Schneider, M. Kamp, S. Maier, S. Höfling, and V. D. Kulakovskii, Circularly polarized light emission from chiral spatially-structured planar semiconductor microcavities, *Phys. Rev. B* **89**, 045316 (2014).
 - [3] S. V. Lobanov, S. G. Tikhodeev, N. A. Gippius, A. A. Maksimov, E. V. Filatov, I. I. Tartakovskii, V. D. Kulakovskii, T. Weiss, C. Schneider, J. Geßler, M. Kamp, and S. Höfling, Controlling circular polarization of light emitted by quantum dots using chiral photonic crystal slabs, *Phys. Rev. B* **92**, 205309 (2015).
 - [4] S. Takahashi, T. Tajiri, Y. Ota, J. Tatebayashi, S. Iwamoto, and Y. Arakawa, Circular dichroism in a three-dimensional semiconductor chiral photonic crystal, *Appl. Phys. Lett.* **105**, 051107 (2014).
 - [5] A. A. Demenev, V. D. Kulakovskii, C. Schneider, S. Brodbeck, M. Kamp, S. Höfling, S. V. Lobanov, T. Weiss, N. A. Gippius, and S. G. Tikhodeev, Circularly polarized lasing in chiral modulated semiconductor microcavity with gas quantum wells, *Appl. Phys. Lett.* **109**, 171106 (2016).
 - [6] K. Konishi, T. Kan, and M. Kuwata-Gonokami, Tunable and nonlinear metamaterials for controlling circular polarization, *J. Appl. Phys.* **127**, 230902 (2020).
 - [7] M. Bernardi, M. Palumbo, and J. C. Grossman, Extraordinary sunlight absorption and one nanometer thick photovoltaics using two-dimensional monolayer materials, *Nano Lett.* **13**, 3664 (2013).
 - [8] A. V. Poshakinskiy, D. R. Kazanov, T. V. Shubina, and S. A. Tarasenko, Optical activity in chiral stacks of 2D semiconductors, *Nanophotonics* **7**, 753 (2018).
 - [9] A. Castellanos-Gomez, M. Buscema, R. Molenaar, V. Singh, L. Janssen, H. S. J. van der Zant, and G. A. Steele, Deterministic transfer of two-dimensional materials by all-dry viscoelastic stamping, *2D Mater.* **1**, 301 (2014).
 - [10] L. Mennel, M. Paur, and T. Mueller, Second harmonic generation in strained transition metal dichalcogenide Monolayers: MoS₂, MoSe₂, WS₂, and WSe₂, *APL Photonics* **4**, 034404 (2019).
 - [11] T. I. Andersen, G. Scuri, A. Sushko, K. De Greve, J. Sung, Y. Zhou, D. S. Wild, R. J. Gelly, H. Heo, D. Bérubé *et al.*, Excitons in a reconstructed moiré potential in twisted WSe₂/WSe₂ homobilayers, *Nat. Mater.* **20**, 480 (2021).
 - [12] See Supplemental Material at <http://link.aps.org/supplemental/10.1103/PhysRevB.105.L241406> for a more extensive the-

- oretical discussion as well as additional measurement data.
- [13] K. Tran, G. Moody, F. Wu, X. Lu, J. Choi, K. Kim, A. Rai, D. A. Sanchez, J. Quan, A. Singh *et al.*, Evidence for moiré excitons in van der Waals heterostructures, *Nature (London)* **567**, 71 (2019).
- [14] K. L. Seyler, P. Rivera, H. Yu, N. P. Wilson, E. L. Ray, D. G. Mandrus, J. Yan, W. Yao, and X. Xu, Signatures of moiré-trapped valley excitons in MoSe₂/WSe₂ heterobilayers, *Nature (London)* **567**, 66 (2019).
- [15] W. Li, X. Lu, S. Dubey, L. Devenica, and A. Srivastava, Dipolar interactions between localized interlayer excitons in van der waals heterostructures, *Nat. Mater.* **19**, 624 (2020).
- [16] F. Wu, T. Lovorn, and A. H. MacDonald, Theory of optical absorption by interlayer excitons in transition metal dichalcogenide heterobilayers, *Phys. Rev. B* **97**, 035306 (2018).
- [17] H. Yu, Y. Wang, Q. Tong, X. Xu, and W. Yao, Anomalous Light Cones and Valley Optical Selection Rules of Interlayer Excitons in Twisted Heterobilayers, *Phys. Rev. Lett.* **115**, 187002 (2015).
- [18] J. Choi, M. Florian, A. Steinhoff, D. Erben, K. Tran, D. S. Kim, L. Sun, J. Quan, R. Claassen, S. Majumder *et al.*, Twist Angle-Dependent Interlayer Exciton Lifetimes in Van Der Waals Heterostructures, *Phys. Rev. Lett.* **126**, 047401 (2021).
- [19] M. Förg, A. S. Baimuratov, S. Yu, Kruchinin, I. A. Vovk, J. Scherzer, J. Förste, V. Funk, K. Watanabe, T. Taniguchi, and A. Högele, Moiré excitons in MoSe₂-WSe₂ heterobilayers and heterotrilayers, *Nat. Commun.* **12**, 1656 (2021).
- [20] E. L. Ivchenko, V. P. Kochereshko, A. Yu. Naumov, I. N. Uraltsev, and P. Lavallard, Magnetic-Field-Effects on photoluminescence polarization in type II GaAs/AlAs superlattices, *Superlattices Microstruct.* **10**, 497 (1991).
- [21] R. I. Dzhioev, H. M. Gibbs, E. L. Ivchenko, G. Khitrova, V. L. Korenev, M. N. Tkachuk, and B. P. Zakharchenya, Determination of interface preference by observation of linear-to-circular polarization conversion under optical orientation of excitons in Type-II GaAs/AlAs superlattices, *Phys. Rev. B* **56**, 13405 (1997).
- [22] S. V. Gupalov, E. L. Ivchenko, and A. V. Kavokin, Fine structure of localized exciton levels in quantum wells, *J. Exp. Theor. Phys.* **86**, 388 (1998).
- [23] H. Yu, G.-B. Liu, P. Gong, X. Xu, and W. Yao, Dirac cones and dirac saddle points of bright excitons in monolayer transition metal dichalcogenides, *Nat. Commun.* **5**, 3876 (2014).
- [24] M. M. Glazov, T. Amand, X. Marie, D. Lagarde, L. Bouet, and B. Urbaszek, Exciton fine structure and spin decoherence in monolayers of transition metal dichalcogenides, *Phys. Rev. B* **89**, 201302(R) (2014).
- [25] Y. Bai, L. Zhou, J. Wang, W. Wu, L. J. McGilly, D. Halbertal, C. F. B. Lo, F. Liu, J. Ardelean, P. Rivera *et al.*, Excitons in strain-induced one-dimensional moiré potentials at transition metal dichalcogenide heterojunctions, *Nat. Mater.* **19**, 1068 (2020).
- [26] L. V. Kotova, A. V. Platonov, A. V. Poshakinskiy, and T. V. Shubina, Polarization conversion in MoS₂ flakes, *Semiconductors* **54**, 1509 (2020).
- [27] A. Mitioglu, S. Anghel, M. V. Ballottin, K. Sushkevich, L. Kulyuk, and P. C. M. Christianen, Anomalous rotation of the linearly polarized emission of bright excitons in strained WSe₂ monolayers under high magnetic fields, *Phys. Rev. B* **99**, 155414 (2019).
- [28] S. A. Tarasenko, Optical orientation of electron spins by linearly polarized light, *Phys. Rev. B* **72**, 113302 (2005).
- [29] S. A. Tarasenko, Thermal orientation of electron spins, *Semiconductors* **42**, 967 (2008).